Environmental Research 208 (2022) 112655

Contents lists available at ScienceDirect

Environmental Research

journal homepage: www.elsevier.com/locate/envres

Removal of gaseous benzene by a fixed-bed system packed with a highly porous metal-organic framework (MOF-199) coated glass beads

Bhaskar Anand [a], Ki-Hyun Kim [a,*], Ravi Kumar Sonwani [b,c], Jan E. Szulejko [a], Philippe M. Heynderickx [d,e]

[a] Department of Civil and Environmental Engineering, Hanyang University, Seoul, 04763, Republic of Korea
[b] Department of Chemical Engineering & Technology Indian Institute of Technology (BHU), Varanasi, 221005, Uttar Pradesh, India
[c] Department of Chemical Engineering, Indian Institute of Petroleum and Energy (IIPE), Visakhapatnam, 530003, Andhra Pradesh, India
[d] Center for Environmental and Energy Research (CEER) – Engineering of Materials Via Catalysis and Characterization, Ghent University Global Campus, 119-5 Songdomunhwa-Ro, Yeonsu-Gu, Incheon, 406-840 South Korea
[e] Department of Green Chemistry and Technology, Faculty of Bioscience Engineering, Ghent University, Coupure Links 653, Ghent, B.9000, Belgium

ARTICLE INFO

Keywords:
Glass bead
Coating
MOF-199
Pressure drop
VOCs removal
Isotherm modeling
Kinetic analysis

ABSTRACT

The utility of nanomaterial adsorbents is often limited by their physical features, especially fine particle size. For example, a large bed-pressure drop is accompnied inevitably, if fine-particle sorbents are used in a packed bed system. To learn more about the effect of adsorbent morphology on uptake performance, we examined the adsorption efficiency of metal-organic framework 199 (MOF-199) in the pristine (fine powder) form and after its binding on to glass beads as an inert support. Most importantly, we investigated the effect of such coatings on adsorption of gaseous benzene (0.1–10 Pa) in a dry N_2 stream, particularly as a function of the amount of MOF-199 loaded on glass beads (MOF-199@GB) (i.e., 0,% 1%, 3%, 10%, and 20%, w/w) at near-ambient conditions (298 K and 1 atm). A 1% MOF-199 load gave optimal performance against a 0.1 Pa benzene vapor stream in 1 atm of N_2, with a two-to five-fold improvement (e.g., in terms of 10% breakthrough volume [BTV] (46 L atm [g. MOF-199)$^{-1}$], partition coefficient at 100% BTV (3 mol [kg.MOF-199]$^{-1}$ Pa^{-1}), and adsorption capacity at 100% BTV (20 mg [g.MOF-199]$^{-1}$ (areal capacity: 8.8 × 10^{-7} mol m^{-2}) compared with those of 3%, 10%, and 20% loading. The relative performance of benzene adsorption was closely associated with the content of MOF-199@GB (e.g., 1% > 3% > 10% > 20%) and the surface availability (m^2 [g.MOF-199]$^{-1}$) such as 291 > 221 > 198 > 181, respectively. This study offers new insights into the strategies needed to expand the utility of finely powdered MOFs in various environmental applications.

1. Introduction

Since the mid-18th century, new and emerging manufacturing techniques have slowly but steadily driven the (Western) industrial revolution (Rosenberg and Birdzell, 1990). This in turn drove prosperity in Western Europe and the U.S. in the 19th century (in a pattern similar to that of South Korea's after the 1960s and modern China in the post-1980s period). In each case, industrialization was accompanied by deteriorating atmospheric conditions and environmental metrics (Ashton, 1997; Perkin, 2003). One of the most harmful group of pollutants in outdoor and indoor air, volatile organic compounds (VOCs) produced and emitted from diverse sources pose significant threats to human health (Serna-Guerrero and Sayari, 2007; Spengler and Sexton, 1983; Wilson, 1968).

To reduce the health risk posed by indoor air pollution, engineers have explored diverse techniques, including adsorption, air ionization, catalysis, photocatalysis, and micro-fuel cells) (Kim et al., 2017; Raza et al., 2017). Adsorption's facile and user-friendly properties have made it a preferred option. Adsorptive removal requires specific characterization of the potential of a given sorbent for each application (Chiang et al., 2001; Gaffney, 1996). Among a variety of adsorbents, metal-organic frameworks (MOFs) are well known for their high adsorption capacity with extremely high surface areas (at the expense of small pore size) of up to approximately 10,000 m^{3}g^{-1} (Farha et al., 2012).

In the laboratory, the full utility of MOF adsorbents has rarely been demonstrated due to physical constraints (e.g., small particle size) in

* Corresponding author.
E-mail address: kkim61@hanyang.ac.kr (K.-H. Kim).

https://doi.org/10.1016/j.envres.2021.112655
Received 18 November 2021; Received in revised form 29 December 2021; Accepted 29 December 2021
Available online 6 January 2022

Glossary of Abbreviations, Acronyms, and Symbols

AC	adsorption capacity
BET	Brunauer–Emmett–Teller
BT	breakthrough
BTV	breakthrough volume
C_{in}	inlet concentration
C_{out}	outlet concentration
FID	flame ionization detector
FTIR	Fourier-transform infrared spectroscopy
GC	gas chromatography
G-WS	gaseous working standard
k_1	rate constant for pseudo-first-order kinetic model
k_2	rate constant for pseudo-second-order kinetic model
LVI	large-volume injector
MDL	method detection limit
MOF	metal-organic framework
MOF-199@GB	metal-organic framework 199 bound on glass beads
PC	partition coefficient
PD	percentage difference
PEA	polyester aluminum
PFOM	pseudo-first-order kinetic model
PS	primary standard
PSOM	pseudo-second-order kinetic model
PXRD	powder X-ray diffraction
Q_{mono}	Brunauer–Emmett–Teller surface monolayer capacity
SV	space velocity
VOC	volatile organic compound
UR	uptake rate

adsorption applications. This is because if a finely powdered MOF is placed in a reactor (e.g., a packed-bed tube) generally suffers from a significant pressure drop along the sorbent bed, significantly lowering the space velocity (SV) (Barea et al., 2014; Khan et al., 2013). Because MOFs are often tested under static conditions in a volumetric apparatus, laboratory-derived data cannot adequately reflect the practical conditions that can pose various hindering factors (e.g., pressure--drop/SV–related issues) (Hu et al., 2019). Stream-flow resistance or mass loss in packed beds can also reduce removal efficiency (Valizadeh et al., 2018).

In the development of the packed-bed adsorption system, it is important to overcome stream-flow restrictions caused by the fine particle size of sorbents (e.g., MOFs). In our previous study, we investigated the efficacy of a denuder system prepared by binding MOFs to the inner surface of a quartz tube (90 mm length with 4 ID × 6 mm) as an alternative to a packed bed sorbent tube (Anand et al., 2020b). The performance of benzene adsorption by the developed denuder was evaluated and compared against a packed-bed tube filled up with MOF sorbent. The superiority of the former was validated to resolve pressure/SV drop issues for nanoscale adsorbents (like MOFs). However, the denuder system showed a considerably lower/limited performance towards benzene removal by 4 to 5-fold than that of packed bed adsorbent (Anand et al., 2020b). In this research, a new attempt has been made to overcome the limitations of adsorption bed packed with fine particle size (simple denuder system (e.g., pressure/SV drop and reduced efficiency). To this end, a new type of packed bed sorbent system has been built by binding the adsorbent MOFs to the outer surface of inert glass beads (0.5 mm) and use them to pack the inner wall of a flow tube instead of finely powdered MOFs. As such, the ability of a new concept of packed bed built as MOF@glass beads (MOF@GB) was explored to capture benzene vapor at the parts-per-million level. Subsequently, MOF-199 was selected for the study as representative MOF due to its facile synthesis and the fact that it is the most well-studied MOF (Szanyi et al., 2012).

Here, we evaluate the performance of MOF-199@GB to learn more about its utility in practical operations. MOF-199 belongs to one of the most studied groups of easily synthesized MOFs. The basic performance (measured by 10% breakthrough volume [BTV_{10}]) of MOF-199@GB against gaseous benzene was assessed as a function of benzene partial pressure (0.1–10 Pa) using a gas standard of 1 atm of dry N_2 balance. The BTV_{10} metric was first assessed at breakthroughs levels of 10%, 50%, 90%, and 100%. Other performance metrics, including adsorption capacity (AC), partition coefficient (PC), and uptake rate (UR), were also calculated at each of the four breakthrough levels. As real-world application of MOFs for dynamic adsorptive removal has yet to be explored in any depth, we tested the viability of MOF-masked glass beads to help expand the applicability of MOF as sorbent media for the removal of VOCs.

2. Materials and methods

2.1. Materials

Copper nitrate (hemi)pentahydrate ($Cu(NO_3)_2$•$2.5H_2O$; 98% purity), 1,3,5-benzenetricarboxylic acid (H_3BTC; 95% purity), polyvinyl alcohol (PVA; MW 146,000–186,000; 87–89% hydrolyzed), ethanol (ETOH; 99% purity), dimethylformamide (DMF; 99% purity), and glass beads (diameter = 0.5 mm) were obtained from Sigma-Aldrich and used as received.

A gaseous working standard (G-WS) for benzene was prepared from a primary standard (PS) of benzene gas (500 ppm) supplied by RIGAS (South Korea). The G-WS was used to examine the adsorption of benzene onto MOF-199@GB under various conditions. In laboratory experiments, the G-WS was prepared at five different concentrations (1, 5, 10, 50, and 100 ppm) by diluting its PS (500 ppm) in ultrapure dry N_2 (99.999%, RIGAS). The prepared G-WS was stored in an 80 L polyester aluminum (PEA) bag (Part No. 205-3001-40, Top Trading Co, South Korea) (equilibration time = 10 min) before experimental use.

2.2. Synthesis of MOF-199

A solvothermal technique was used to prepare a MOF following the procedures of our previous studies (Dutta et al., 2018a). Briefly, 4 g (17.2 mmol) of $Cu(NO_3)_2$•$2.5H_2O$ and 2 g (9.5 mmol) of H_3BTC precursors were solubilized together in 100 mL of a mixture of DMF, ethanol, and water at a volume ratio of 1:1:1. The reaction mixture was then transferred to a polytetrafluoroethylene-lined stainless-steel autoclave reactor (150 mL), tightly capped, and heated at 85 °C for 20 h in a hot air oven (ED-CO150, Hanyang Scientific Equipment Co, Ltd, South Korea). The reactor contents were transferred to two different 50 mL Falcon polypropylene conical tubes (Corning Science, Mexico). Later, each Falcon tube was centrifuged at 2000 rpm for 10 min (Hanil Science Industrial Co. Ltd, South Korea) to separate the supernatant (solvent) and solids (blue crystals). The blue crystals were subsequently washed twice with 25 mL of DMF to remove the unreacted organic linker. The resulting product was submersed in DMF (25 mL) for 24 h to remove impurities. The product was separated using a centrifuge (Hanil Science Industrial Co. Ltd, South Korea). Finally, the precipitated product was kept in an oven at 170 °C for 24 h and then stored in a tightly closed glass vial for later characterization and future use.

2.3. Preparation of MOF-199@GB

For the preparation of MOF-199@GB, we used commonly available laboratory equipment, including 5 mL single-channel pipettes (Eppendorf, Germany), 150 mL Pyrex glass beakers (Corning Inc, USA), stirring

rods, and spatulas. Prior to coating the MOF, a binder solution was prepared by dissolving 2 g of PVA in 30 mL of water and setting it aside for 6 h. To make a uniform PVA solution, the mixture was sonicated for 45 min. To prepare the 1% MOF-199@GB, 9.9 g of glass beads were put into a 150 mL Pyrex glass beaker to which 0.5 mL of PVA solution (PVA/water: 0.066 g mL^{-1}) was added using a single-channel pipette. The mixture was stirred manually using a glass rod to coat the glass beads with PVA. Next, 0.1 g of MOF-199 (i.e., 1% MOF-199 w/w loading) was sprinkled onto PVA-coated glass beads and then manually mixed with a glass rod for 5 min. Finally, the MOF-199–coated glass beads were transferred to a Petri dish and dried at 80 °C in a hot air oven (Fig. 1). The fractional MOF-199/PVA/GB composition is provided in Table 1. Two-dimensional schematics of the MOF-199@glass bead are shown in Fig. 2 (For details on sorbent bed packing, see section 2.5.).

2.4. Characterization

Th physiochemical properties (crystal structure, thermal stability, chemical functionality, porosity, and morphological features) of the prepared MOF-199 and MOF-199@GB were determined by a variety of techniques. Crystallinity and main phases of the synthesized MOF-199 were investigated using powder X-ray diffraction (PXRD, Bruker, D8 Advance) over a 2θ range of 5°–50°. Fourier-transform infrared spectroscopy (FTIR, Spectrum Two, PerkinElmer) was used to investigate the surface functionalities of MOF-199 in a spectral range of 400–4000 cm^{-1}. The surface morphology of the prepared MOF-199 and MOF-199@GB was assessed using scanning electron microscopy (SEM, Thermo Scientific, Verios G4 UC). Pore texture properties were calculated based on the N_2 adsorption-desorption isotherm at 77 K obtained with a Micromeritics (3 Flex) surface area analyzer. Their specific surface areas and pore-size distributions were determined using Brunauer–Emmett–Teller (BET) and Barret–Joyner–Halenda methods, respectively. All pores of the adsorbent were filled with N_2 (at $P\ P_o^{-1} = 0.9$) to yield their total pore volume. The thermal durability of MOF-199 and MOF199@GB were investigated using a TGA7 thermogravimetric analysis (TGA) apparatus (PerkinElmer) over a temperature range of 0°C – 1000°C (heating ramp: 10°C min^{-1}, N_2 flow = 100 mL atm min^{-1}).

2.5. Sorbent bed packing

To prepare a packed bed for adsorption experiments, a quartz sorbent tube sampler (internal diameter = 4 mm and length = 9 cm; Model No. 002-11001-90, Top Trading Co, South Korea) was packed with 50 mg of MOF-199@GB. These sorbent materials were packed centrally and held in place by quartz wool plugs at both ends of the sorbent bed. The plugs have a negligible sorption capacity for benzene (Khan et al., 2018). The sorbent tubes were stored after being sealed by Teflon caps when not in use. Prior to use, the sorbent tubes were placed in a sorbent tube conditioner (CT2000 Tube Cleaner, Kemtec Ins Co, South Korea) for thermal conditioning at 150 °C for 3 h under continuous purging by ultrapure (99.999%) N_2 at a flow rate of 0.2 L min^{-1}. This step removed or reduced pre-adsorbed pollutants and impurities from the adsorbent.

2.6. Benzene adsorption experiment

The adsorption efficacy of benzene (in gaseous streams) onto MOF-199@GB was investigated using five concentrations of gaseous benzene (1, 5, 10, 50, and 100 ppm). We evaluated the effect of MOF-199 loading (1%, 3%, 10%, and 20%, w/w) on glass beads in the adsorptive removal of benzene molecules. A large-volume injector (LVI) interfaced with a gas chromatograph equipped with a flame ionization detector (GC-FID) was used for near-real-time monitoring of the adsorptive interaction between the adsorbent bed and gaseous benzene (Anand et al., 2020a). Automated collection of the exiting VOC samples was carried out to measure the outlet stream concentration at five different flushing event times: (i) very short (0.1 min), (ii) short (0.5 min), (iii) medium (1.5 min), (iv) long (3 min), and (v) ultra-long (5 min). The duration of flushing intervals increased with loaded-stream volume in steps to acquire temporally balanced data points in the progress of BT. The flushing event sequence used in the present experiment is shown as a flow chart (Fig. 1S).

2.7. Analysis of benzene adsorption using an LVI-GC-FID

The concentration of the target VOC (benzene) in the sorbent tube outlet stream was determined by an LVI-GC-FID equipped with an automated large volume injection system. The operational conditions of the LVI-GC-FID are summarized in Table 1S. Numerical integration via the trapezoid rule was used to construct a sorption isotherm from the raw chromatogram peak area using the response factor for calibration of the inlet stream and Eq. (1) (Khan et al., 2018):

$$m_{tot} = \sum_{i=1}^{n} \Delta m_i = \sum_{i=1}^{n} \left[C_{in} - \frac{[A]_{i-1} + [A]_i}{2} \right] \cdot \Delta V_i \quad (1)$$

where M_{tot} is the mass sorbed (mg) in the ith run, C_{in} is the inlet concentration (mg L^{-1}) (from the one-point response factor), ΔV_i is the loaded volume (L) per run for the ith run, i is the run number, and [A] is the concentration of analyte according to Eq. (2):

$$[A] = \frac{\text{peak area}}{\text{response factor}}. \quad (2)$$

The breakthrough in the ith run was the ratio of the outlet and inlet

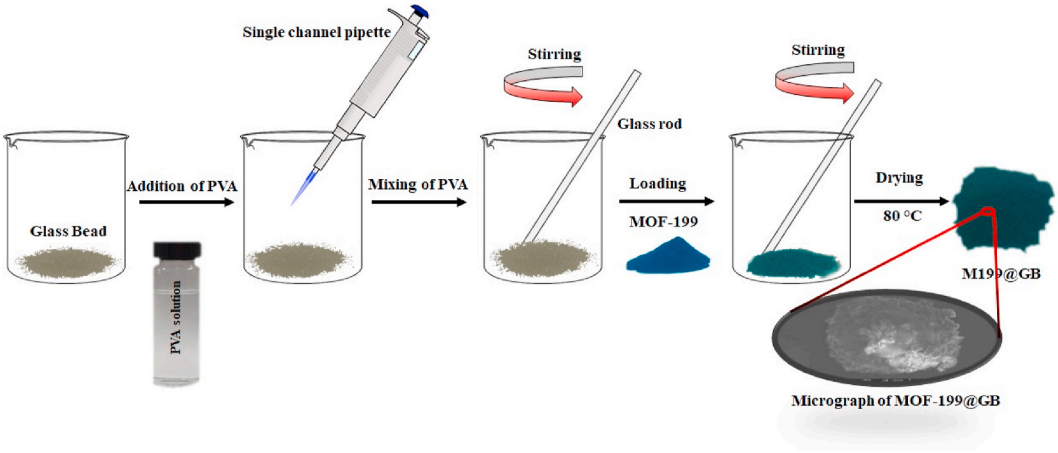

Fig. 1. Schematic of the preparation procedures for MOF-199@GB.

Table 1
The proportional composition of glass beads, PVA, and MOF-199 (active sorbent) in different variants of MOF-199@GB along with a summary of the pore texture analysis of MOF-199@GB.

Order	Name	Mass of glass bead	Volume of PVA	Mass of active sorbent	Percentage of active sorbent	BET of MOF-199@GB	BET of active sorbent	Pore volume of MOF-199@GB	Pore volume of active sorbent	Pore size
		g	mL	g	%	$m^2\ g^{-1}$	m^2 (g.MOF-199)$^{-1}$	$cm^3\ g^{-1}$	cm^3 (g.MOF-199)$^{-1}$	Å
1	1% MOF-199@GB	9.9	0.50	0.10	1	2.9	291	0.00071	0.071	14.6
2	3% MOF-199@GB	9.7	0.60	0.30	3	6.6	221	0.00092	0.031	12.9
3	10% MOF-199@GB	9.0	0.80	1.0	10	19.8	198	0.00290	0.029	12.8
4	20% MOF-199@GB	8.0	1.0	2.0	20	36.1	181	0.00756	0.038	14.1
5	Pristine MOF-199				100		1212		0.450	15.0

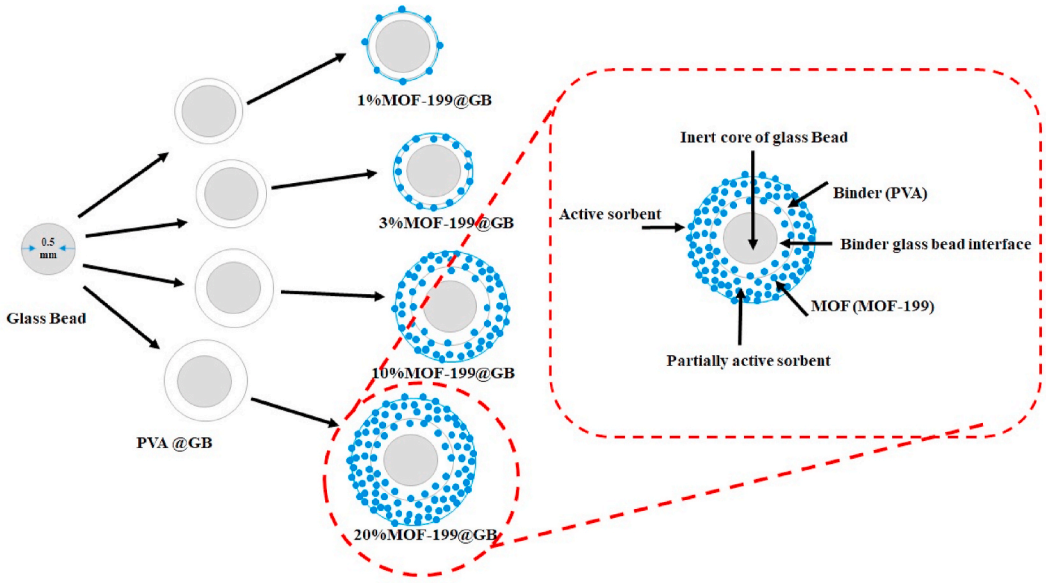

Fig. 2. A two-dimensional view of MOF-199@GB.

benzene concentrations (C_{out}/C_{in}). The outlet concentration was estimated by averaging the observed concentration in the ith and (i-1)th runs, as shown in Eq. (3):

$$\frac{C_{out}}{C_{in}} = \frac{\frac{[A]_{i-1}+[A]_i}{2}}{C_{in}} \quad (3)$$

The AC was calculated by using:

$$AC = \frac{m_{tot}}{m_{ad}} \quad (4)$$

where the total mass (m_{tot}; mg) of benzene is taken up by an adsorbent of mass (m_{ad}; g) loaded on glass beads in the packed bed.

The concept of a PC, in mol kg^{-1} Pa^{-1}, has been employed to assess the magnitude of solvation of a solute in two immiscible phases and judge the importance of solute-solute or solute-solvent interactions (Leo et al., 1971). According to Henry's law, a PC is independent of concentration if there are no solute-solute or solute-solvent interactions (Leo et al., 1971), as in Eq. (5):

$$(PC) = \frac{Adsorption\ capacity\ (at\ n\%\ breakthrough)}{Outlet\ concentration\ (at\ n\%\ breakthrough)} \quad (5)$$

where the AC (mol kg^{-1}) is the concentration of a solute in the absorbent and the outlet concentration is described as the partial pressure (in Pa) of the solute in the gas phase. The PC is measured in mol kg^{-1} Pa^{-1}.

The UR (g kg^{-1} h^{-1}) of benzene vapor by the MOF-199–coated glass beads can be computed using Eq. (6):

$$(UR) = \frac{M(sorb)}{Sorbent\ mass\ \mathrm{x}\ Purging\ time} \quad (6)$$

where the mass sorbed per run (M_{sorb}; g) is the amount of benzene taken up by the adsorbent during a particular run while the sorbent mass (kg) is the amount of adsorbent loaded on glass bead. In the present study, the LVI-GC-FID operated in automated flushing mode. The operating parameters of the LVI-GC-FID are provided in Table 1S. Automatic flushing was regulated according to the purging sequence visualized in Fig. 1S.

An extrapolation method (cubic B-spline) using the Origin Pro 2016 data-analysis software was employed to estimate the 100% breakthrough using boundary constraints (e.g., capacity cannot be infinite) (Anand et al., 2021). This 100% breakthrough was used to determine the corresponding adsorption performance metrics of maximum AC, PC, and UR.

Table 2
Summary of performance metric for benzene adsorption onto MOF-199@GB.

Order	Concentration	BTV10	BTV50	BTV90	BTV100	AC at BTV10	AC at BTV50	AC at BTV90	AC at BTV100	PC at BTV10	PC at BTV50	PC at BTV90	PC at BTV100	UR at BTV10	UR at BTV50	UR at BTV90	UR at BTV100
	ppm	L atm (g.MOF-199)$^{-1}$				mg (g.MOF-199)$^{-1}$				mol (kg.MOF-199)$^{-1}$Pa^{-1}				g (kg.MOF-199)$^{-1}$ h^{-1}			
A. Adsorption performance of 1% MOF-199@GB for benzene adsorption onto active sorbent 0.5 mg																	
1	1	46	108	20000	38000	0.1	0.1	0.2	20	0.06	0.06	1.00	3.00	91	74	10	0.2
2	5	20	96	1058	34000	0.3	0.5	1.0	23	0.07	0.06	0.10	1.00	452	369	26	7.0
3	10	10	86	1220	16800	0.7	0.8	8.0	25	0.06	0.05	0.11	0.20	853	740	118	2.0
4	50	7	80	854	10800	2.3	4.0	25.0	50	0.05	0.04	0.07	0.10	3955	3191	661	57.0
5	100	5	60	696	6000	3.8	17.3	59.0	66	0.04	0.05	0.12	0.40	8585	6829	1237	790.0
B. Adsorption performance of 3% MOF-199@GB for benzene adsorption onto active sorbent 1.5 mg																	
1	1	27	513	2667	4947	0.1	1	3	3	0.11	0.20	0.40	0.33	38	21	4	1.0
2	5	20	433	1113	4267	0.3	4	6	7	0.08	0.21	0.20	1.76	187	102	20	2.6
3	10	17	260	2600	4000	1.0	5	19	22	0.05	0.13	0.30	0.27	356	210	42	3.2
4	50	13	100	1133	1933	2.0	10	40	47	0.04	0.05	0.11	0.11	1758	1029	202	46.0
5	100	7	93	580	1800	3.0	14	46	60	0.03	0.03	0.06	0.08	3284	2059	420	59.0
C. Adsorption performance of 10% MOF-199@GB for benzene adsorption onto active sorbent 5 mg																	
1	1	7.8	150	1320	4600	0.1	0.3	1	2	0.030	0.060	0.14	0.19	11	6	1	0.0
2	5	3.4	96	1200	3000	0.2	1.0	4	5	0.026	0.050	0.11	0.13	57	30	6	0.5
4	10	3	32	960	2000	0.3	1.1	8	9	0.018	0.020	0.11	0.12	110	65	13	0.6
4	50	2.6	18.4	500	1720	0.4	2.0	14	26	0.110	0.010	0.04	0.06	500	315	60	1.0
5	100	2.2	14.8	460	1280	1.0	27.0	37	40	0.009	0.008	0.04	0.04	987	651	154	10.0
D. Adsorption performance of 20% MOF-199@GB for benzene adsorption onto active sorbent 10 mg																	
1	1	9.9	480	1368	3800	0.04	1.0	2	2	0.014	0.250	0.22	0.24	6	3	1	0.002
2	5	7	84	800	2500	0.10	2.0	3	5	0.010	0.040	0.09	0.11	27	16	8	0.800
3	10	2	380	800	2000	0.50	1.0	6	8	0.012	0.020	0.08	0.10	53	31	6	1.000
4	50	1.3	7.3	560	1500	0.70	6.0	19	24	0.003	0.010	0.05	0.06	213	142	30	2.000
5	100	0.54	6.4	305	1600	0.90	1.0	20	32	0.002	0.003	0.03	0.04	416	240	61	6.000

2.8. Quality assurance and quality control

For the quality assurance (QA) of VOC quantitation made in this work, five-point calibrations for LVI-GC-FID (at 1, 5, 10, 50, and 100 ppm) were carried out based on the fixed standard volume method (Kim and Nguyen, 2007; Pandey and Kim, 2009). The calibration generally exhibits excellent linearity for LVI-GC-FID ($R^2 = 0.999$; mass range = 1.59–318 ng). The method detection limit (MDL) and relative standard error (RSE) were also calculated as part of QA (Table 2S). The latter was 1.01% and the former was 0.13 ng. As a control, a packed bed with 500 mg of virgin glass beads was prepared and tested against benzene at a concentration of 10 ppm. The packed bed with virgin glass beads demonstrated instantaneous (100%) breakthrough, indicating that the virgin glass beads were effectively inert against gaseous benzene without any appreciable adsorption capacity for benzene.

3. Results and discussion

3.1. Characterization of MOF-199 and MOF-199@GB

Powder XRD was used to assess the crystalline purity and phases present in the MOF-199 prepared in this study. Fig. 2S(a) compares the PXRD diffraction patterns to those simulated theoretically. A total of 11 major peaks with 2θ values of 6.7°, 9.5°, 11.6°, 13.4°, 14.6°, 17.4°, 19°, 23°, 24°, 25.9°, and 29.4° corresponded to the lattice planes of (200), (220), (222), (400), (331), (333), (440), (444), (551), (662), and (751), respectively (Ahmed et al., 2014; Minh et al., 2018). The Mercury software (CSD Release: 2020, Update 3) was used to visualize and analyze the crystal structures using crystallographic information files (CIF) from the Cambridge Crystallographic Data Centre (CCDC, 2021; Macrae et al., 2020; Xiang et al., 2009). The PXRD patterns of the prepared MOF-199 closely matched those simulated previously (Xiang et al., 2009). Additionally, the 2D (chemical) and 3D (graphical) structural models of MOF-199 were also simulated (using an open-source Java viewer for chemical structures in 3D: JMOL) from CIF files obtained by Cambridge Crystallographic Data Centre (Fig. 3). The FTIR spectra in Fig. 2S(b) of fresh (before adsorption) and spent (after adsorption) MOF-199 samples were used to assess possible changes in chemical functionality due to benzene uptake. The appearance of broad and weak peaks at 3335 and 3347 cm^{-1} in both samples indicates the presence of coordinating water molecules with stretching vibrations of O–H molecules (Morita et al., 2014). The three distinct peaks at 1640, 1447, and 1370 cm^{-1} confirm asymmetric and symmetric stretching vibrations of the carboxylate group in H_3BDC (Vikrant et al., 2019). The spent MOF-199 has three similar peaks at 1645, 1448, and 1372 cm^{-1}. The bending modes of C–H (in- and out-of-plane) of benzenetricarboxylate ($C_9H_3O_6$) can be assigned to the 1107 and 937 cm^{-1} peaks, respectively (Vellingiri et al., 2017). For the spent MOF-199, similar absorption bands at 1109 and 937 cm^{-1} are also obtained. The stretching vibrations of the C–O–Cu coordination bond in the fresh MOF-199 are primarily responsible for the prominent peaks at 732 and 728 cm^{-1} (Anand et al., 2020b). After adsorption, the two peaks at 730 and 728 cm^{-1} can be attributed to stretching vibrations of the C–O–Cu coordination bond. The presence of adsorbed benzene is also reflected in the slight change in FTIR bands. Based on a comparison of FTIR spectra for fresh and spent MOF-199, we inferred that the surface functionality of MOF-199 underwent no significant change due to the adsorption of benzene.

The SEM images (Fig. 3S) show that both MOF-199 and MOF-199@GB maintained an octahedral shape, with average sizes of 10–50 μm. As shown in Fig. 3S(a-i), the SEM micrographs of both forms reveal no major morphological changes in MOF due to the GB coating. However, accumulation and/or aggregation of MOF-199 crystals over the GB substrate is evident in the micrographs of MOF-199@GB, as shown in Fig. 3S(a-h). SEM observations also suggest the extent of accumulation and/or aggregation of MOF-199 due to the coating.

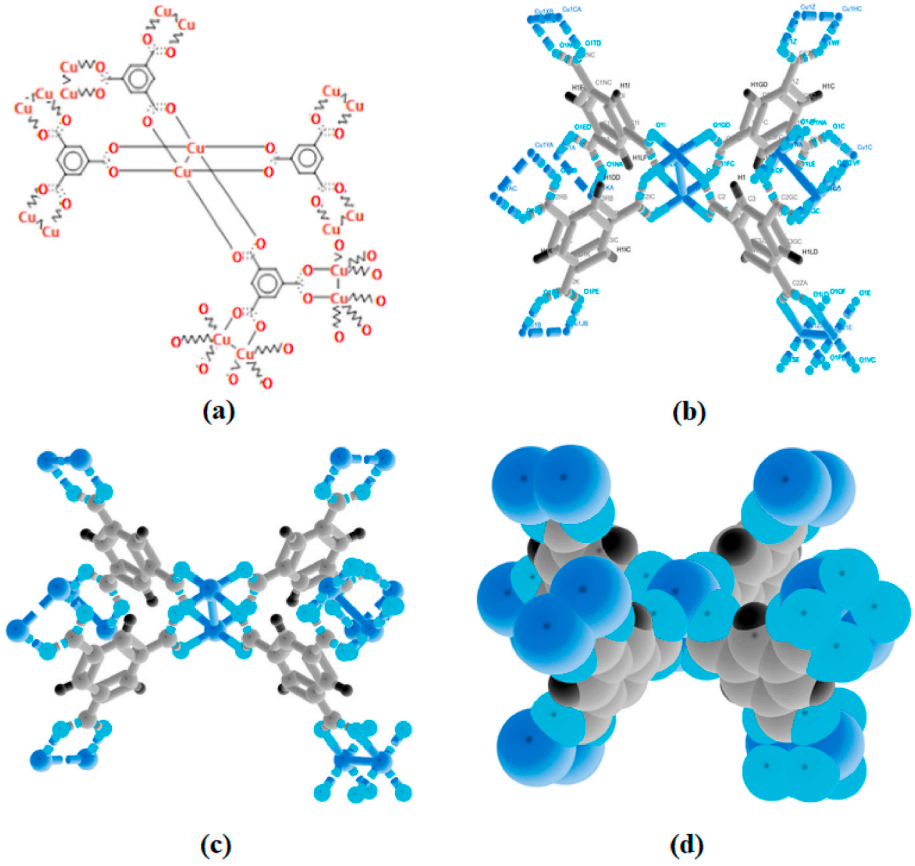

Fig. 3. Graphical structure representation of MOF-199: (a) chemical, (b) capped sticks, (c) ball and sticks, and (d) space fill.

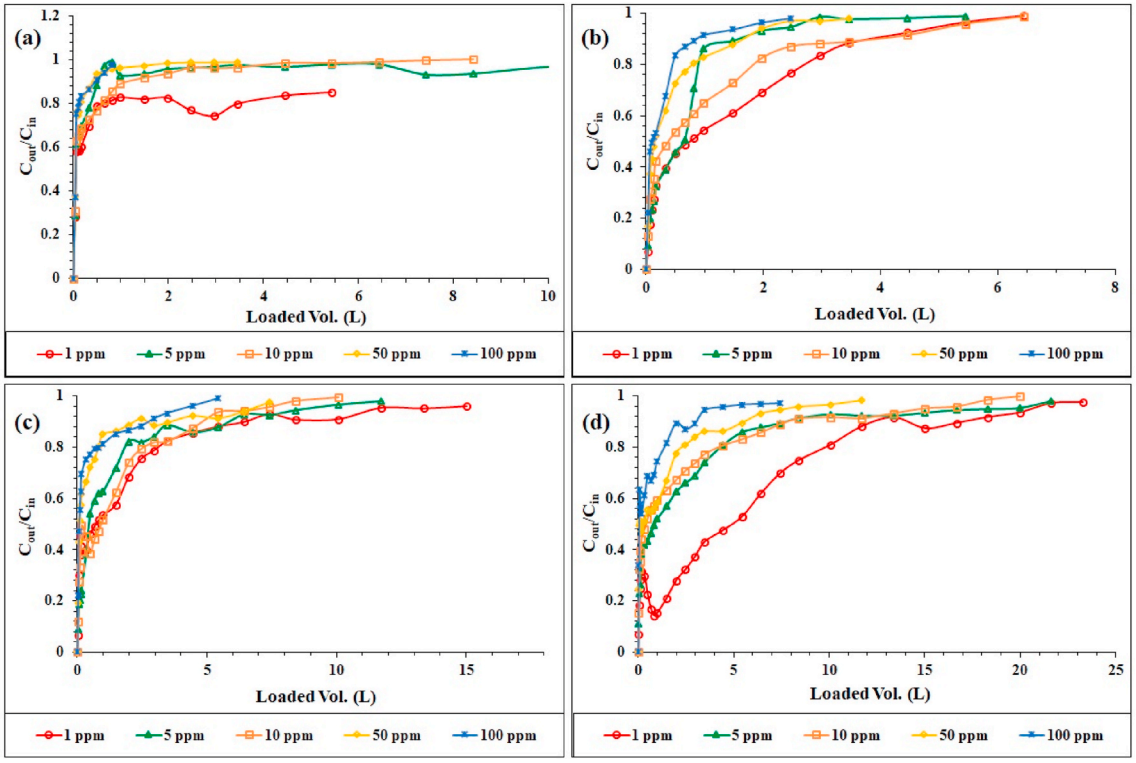

Fig. 4. Breakthrough profiles for different concentrations of benzene (1–100 ppm) adsorption onto MOF-199@GB: (a) 1% MOF-199@GB, (b) 3% MOF-199@GB, (c) 10% MOF-199@GB, and (d) 20% MOF-199@GB.

According to the N_2 adsorption-desorption isotherm analysis (as shown in inset of Fig. 4S), the BET surface of pristine MOF-199 was 1212 m^2 g^{-1}, the total pore volume was 0.45 cm^3 g^{-1}, and the average pore size was 15 nm (microporous). These results are consistent with those of previous reports (Fan et al., 2019). All MOF-199@GB showed a type I isotherm with an apparent hysteresis loops, revealing that the N_2 adsorption mechanism was dominated primarily by capillary condensation indicative of microspores (Zhang et al., 2012). All MOF-199@GBs have relatively small BET surface areas of between 291 and 181 m^2 (g. MOF-199)$^{-1}$ compared with pristine MOF-199 (Table 1). This reduction in surface area can be attributed to alteration of the pore-texture properties of MOF-199 due to interactions with the binder (PVA) (Anand et al., 2020b). The BET analysis also indicated a decrease in the surface area of MOF-199 with increasing incorporation of MOF-199 with GB.

The TGA profile of pristine MOF-199 (as shown in the inset of Fig. 5S) reveals a gradual loss of mass of 34% up to a temperature of 283 °C due to the liberation of weakly bound volatile guest species such as DMF and other solvents. However, in case of MOF-199@GB (Fig. 5S), preliminary mass losses of 0.25%, 0.75%, 1.8%, and 2.2% were observed up to a temperature of 283 °C for 1%, 3%, 10%, and 20% MOF-199@GB, respectively (Andrew Lin and Hsieh, 2015). Such variations can be attributed to differences in the actual proportion of MOF mass incorporated into the glass beads and/or thermal stability of the beads up to 1400–1600 °C (Kothiyal et al., 2012). A sharp weight-loss regime (by another 34%) was also observed with increases in temperature from 283 to 364 °C due to the escape of strongly bounded solvent molecules (Dutta et al., 2018b). Framework collapse (i.e., CuO as an end product) of MOF-199 was accompanied by the liberation of such solvent molecules coordinated with the Cu (II) centers. In the case of MOF-199@GB, weight losses of 0.3%, 0.9%, 2.4%, and 4% were observed for 1%, 3%, 10%, and 20%, respectively.

3.2. Flow constriction and pressure drop assessment

To address the significance of this study in a more organized manner, a study of flow constriction was conducted by pulling 1 L atm of N_2 at an apparent volumetric flow rate of 330 mL min^{-1} through packed beds of pristine MOF-199 and 1% MOF-199@GB. An evacuation time for 1 L atm of N_2 was observed and used to estimate the drop in flow rate. The flow results are summarized in Table 3S. The flow-rate drop was plotted against the loaded mass of MOF-199 to estimate the dependence of the mass flow rate (cm^3 atm s^{-1}) and flow constriction in packed beds of both pristine MOF-199 and 1% MOF-199@GB. The flow-rate drop in the packed bed with pristine MOF-199 was 0.03 cm^3 atm s^{-1} mg^{-1} (Fig. 6S).

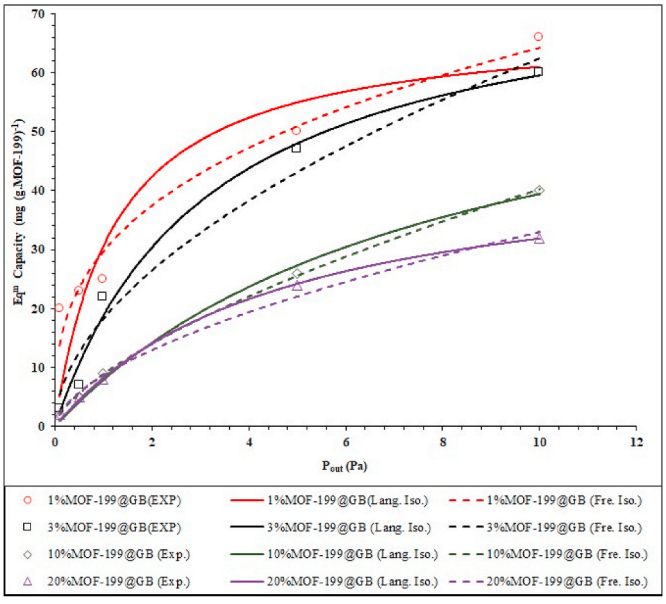

Fig. 5. Non-linear isotherm models (i.e., Langmuir and Freundlich) fitting plots for adsorption of benzene onto MOF-199@GB.

The pressure drop (ΔP) across both packed beds was estimated using the Ergun equation (Eq. (7)) (Ergun, 1952):

$$\Delta P = \frac{150\mu L}{D_p^{\,2}} \frac{(1-\varepsilon)^2}{\varepsilon^3} v_s + \frac{1.75 L\rho}{D_p} \frac{(1-\varepsilon)}{\varepsilon^3} v_s^2 \quad (7)$$

where L is the length of the packed bed, D_p is the equivalent spherical diameter of the packing, ρ is the density of fluid, μ is the dynamic viscosity of the fluid, v_s is the superficial velocity (i.e., the velocity of the fluid if passing through the empty tube at the same volumetric flow rate), and ε is the void fraction (porosity) of the bed.

The estimated pressure drop (ΔP) in a packed bed with pristine MOF-199 (0.1 g) was estimated to be 63.2 kPa (62.4% atm), whereas the packed bed with 1% MOF-199@GB (0.1 g. MOF-199) experienced relatively low levels of pressure drop of 18.6 kPa (18.4% atm). These outcomes suggest the superiority of 1% MOF-199@GB with its four-fold (18.4% atm) reduction in pressure drop.

3.3. Breakthrough assessment

For each of the tested MOF-199@GB, dynamic breakthrough profiles of benzene drawn against the feeding concentration levels of benzene (1–100 ppm) are presented in Fig. 4. The magnitude of the BTV for each MOF-199@GB (MOF-199 = 1%, 3%, 10%, and 20%) decreases with increasing benzene concentrations in the inlet stream. Table 2 summarizes the computed values of the performance metrics, including BTV (L atm [g.MOF-199]$^{-1}$), AC (mg [g.MOF-199]$^{-1}$), PC (mol [kg.MOF-199]$^{-1}$ Pa^{-1}), and UR (g [kg.MOF-199]$^{-1}$ h^{-1}) of MOF-199@GB (MOF-199 = 1%, 3%, 10%, and 20%) at respective varying breakthrough levels (10%, 50%, 90%, and 100%).

At all tested benzene concentrations, the efficiency of benzene adsorption onto MOF-199@GB decreases with increasing MOF-199 loading onto glass beads, in the order 1% < 3% < 10% < 20% (Table 2). This reduction in benzene adsorption (1% > 3% > 10% > 20%) with increased MOF-199 loading onto GB may reflect the effect of the decreasing surface area (m^2 [g.MOF-199]$^{-1}$) such as 291 > 221 > 198 > 181, respectively). The BTV_{10} values for benzene onto MOF-199@GB decreases with increasing inlet concentrations of benzene. For example, in the case of 1% MOF-199@GB, the BTV_{10} values for 1 < 5 < 10 < 50 < 100 ppm of gaseous benzene were 46 > 20 > 10 > 7 > 5 L atm (g.MOF-199)$^{-1}$. Similar patterns were observed for the other three MOF-199@GB adsorbents (MOF-199 = 3%, 10%, and 20%). On the contrary, if the trend in benzene concentration had obeyed Henry's law as an ideal gas, then the BTV_{10} would have been constant and independent of inlet stream concentrations (Langmuir, 1918). Here, the reduction in BTV10 values on increasing inlet concentrations can be attributed to a mass-transfer resistance-based driving force (Moyo et al., 2017). An elevated concentration of benzene in the gaseous stream should lead to rapid filling of available vacant adsorption sites of the adsorbent and quickly develop a mass-transfer resistance in a solid-phase MOF-199@GB adsorbent (Mohan et al., 2009). For a fixed concentration of benzene (1 ppm), the BTV_{10} decreased from 46 to 9.9 L atm (g.MOF-199)$^{-1}$ with an increasing MOF-199 loading on glass beads of 1%–20% in MOF-199@GB. This decrease in BTV_{10} can be attributed to the accumulation and/or aggregation of MOF-199 crystals followed by a reduction in pore entrances available for adsorption.

The AC (mg [g.MOF-199]$^{-1}$) and UR (g [kg.MOF-199]$^{-1}$ h^{-1}) at BTV_{10} increased with increasing inlet concentrations of benzene. Typically, the adsorption capacities for gaseous benzene adsorption by 1% MOF-199@GB at BTV_{10} were in the order of 0.1 < 0.3 < 0.7 < 2.3 < 3.8 mg (g.MOF-199)$^{-1}$, when inlet benzene was applied at 1 < 5 < 10 < 50 < 100 ppm. Likewise, the UR also had similar pattern 91 < 452 < 853 <

Table 3
Summary of the non-linear fitting results of isotherm models (i.e., Langmuir with parameters K_L and Q_m, and Freundlich with parameters K_F and n) for adsorption of benzene onto MOF-199@GB.

Order	Adsorbent	Q_e (mg (g.MOF-199)$^{-1}$)	K_L (Pa^{-1})	Q_m (mg (g.MOF-199)$^{-1}$)	K_F (mg (g.MOF-199)$^{-1}$ $Pa^{-1/n}$)	n	R^2	PD (%)
1	1% MOF-199@GB	66	0.811 ± 0.035	68.5 ± 6.8	29.72 ± 1.37	2.989 ± 0.034	0.809	10
							0.960	2
2	3% MOF-199@GB	60	0.317 ± 0.058	78.3 ± 2.6	18.28 ± 1.04	1.875 ± 0.087	0.990	5
							0.971	15
3	10% MOF-199@GB	40	0.125 ± 0.078	70.8 ± 1.9	8.88 ± 0.07	1.524 ± 0.891	0.995	16
							0.999	2
4	20% MOF-199@GB	32	0.215 ± 0.122	46.7 ± 0.7	8.66 ± 0.34	1.722 ± 0.841	0.998	11
							0.991	7

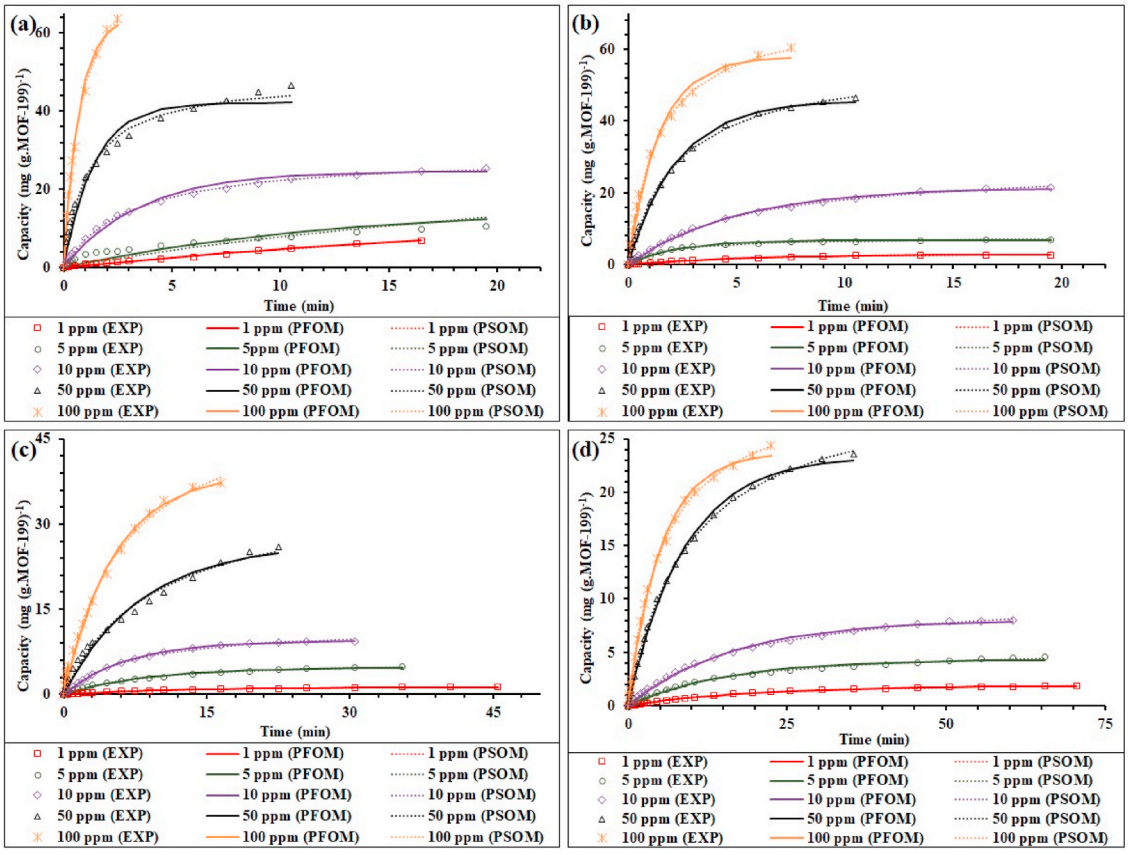

Fig. 6. Kinetic fitting plots (PFOM and PSOM) for adsorption of benzene (1–100 ppm) onto MOF-199@GB: (a) 1% MOF-199@GB, (b) 3% MOF-199@GB, (c) 10% MOF-199@GB, and (d) 20% MOF-199@GB.

3966 < 8585 g (kg.MOF-199)$^{-1}$ h^{-1} for 1–100 ppm, respectively. Similar adsorption patterns of benzene were observed on three other MOF-199@GBs (MOF-199 = 3%, 10%, and 20%). The capacity for benzene adsorption (100 ppm) onto MOF-199@GB at BTV_{10} also decreased from 3.8 to 0.9 mg (g.MOF-199)$^{-1}$ with an increasing MOF-199 loading of 1%–20% in MOF-199@GB. This decrease in capacity can be attributed to the accumulation and/or aggregation of MOF-199 crystals followed by a reduction in surface area available for adsorption, along with channeling of the void space generated in the packing of glass beads. This channeling can be reduced by optimizing the size of glass beads.

As an valuable performance metric, a PC can describe the degree of partitioning of a target analyte (between gas and solid adsorbent phases) at a given loading state (Speight, 2018). A PC value (for example, at BTV_{10}) is considered a less-biased metric (through the normalization of loaded mass of benzene — or any target pollutant — in the packed bed) for evaluating the adsorption efficiency compared with the commonly used AC (Szulejko et al., 2019). As summarized in Table 2, the equilibrium PC values at 100% breakthrough decrease from 0.06 to 0.043 mol (kg.MOF-199)$^{-1}$ Pa^{-1} as the inlet G-WS benzene concentrations increases from 1 to 100 ppm. The reduction in PC values with increasing concentration exhibit an inverse proportionality with the partial pressure of the analyte (Ross, 2012). Overall, the promising performance of benzene adsorption onto MOF-199@GB is based on the interactions between adsorbate and active sorbent (MOF-199). Such strong (electrostatic) interaction is explained at least partially by the presence of open metal sites in the framework (Fig. 3 (a)). MOF-199 has the highest density of Cu···Cu motifs of any known MOF. The exposed coordination sites should provide a high metal-to-unit cell ratio, making MOF-199 an excellent adsorbent for the uptake of gaseous benzene (Hendon and Walsh, 2015).

3.4. Isotherm analysis of benzene adsorption onto MOF-199@GB

Adsorption is often analyzed in terms of equilibrium vapor uptake isotherms (Al-Ghouti and Da'ana, 2020). An appraisal based on

equilibrium AC can shed light on the technical aspects of the adsorption mechanism (Foo and Hameed, 2010). Here, we evaluated the retention or concentration of the adsorbate (benzene) onto an adsorbent (MOF-199@GB) using benzene vapor at a different partial pressure of G-WS and a constant temperature (298 K). Langmuir and Freundlich isotherm models were solved non-linearly to describe the equilibrium adsorption of benzene on the MOF-199@GB (for details of the data analysis, see section 2.7). The Langmuir model, given in Eq. (8), is generally preferred due to its simplicity and the insightful theoretical perspective in the background (Foo and Hameed, 2010). Three indispensable propositions of the Langmuir isotherm are monolayer coverage, the equivalence of adsorption site, and independence of lateral interaction between adsorbate molecules (Langmuir, 1918):

$$Q\,(P) = \frac{Q_m K_L P}{1 + K_L P} \tag{8}$$

where Q_m (mg g^{-1}) is the equilibrium AC and K_L (Pa^{-1}) represents the Langmuir sorption equilibrium constant. If P is small, the Langmuir isotherm converges to Henry's law ($Q(P) = q_m.K_L.P$).

The Freundlich model is generally employed to describe single-component adsorption equilibria on heterogeneous surfaces (Quiñones and Guiochon, 1996). The Freundlich equation (Equation (9)) is obtained by presuming that the extent of reduction of unoccupied active sites by the adsorbate molecules is proportional to a certain power of the partial pressure of the adsorbate (Freundlich, 1932). The adsorbent surface has assorted active sites for adsorption with a dissimilar affinity for the adsorbate in the gaseous stream to induce multi-layer adsorption (Holford, 1982):

$$Q\,(P) = K_F P^{\frac{1}{n}} \tag{9}$$

where K_F (mg g^{-1} $Pa^{-1/n}$) is the Freundlich sorption equilibrium constant, P (Pa) represents the equilibrium pressure, and n is the Freundlich exponent; if n = 1, the equation becomes Henry's law.

Percentage difference (PD) was estimated for contrasting differences between the experimental capacity and the theoretically estimated capacity for each isotherm model (Anand et al., 2021):

$$PD\,(\%) = 100\left(\frac{Q_{EXP} - Q_{EST}}{Q_{EXP}}\right) \tag{10}$$

where Q_{EXP} and Q_{EST} are the experimental and predicted adsorption capacities (mg g^{-1}) estimated theoretically by the studied models, respectively.

Table 3 compares the Langmuir model (R^2: 0.809–0.998; PD: 5%–16%) with the Freundlich isotherm (R^2: 0.96–0.999; PD: 2%–15%), with the latter showing a better fit to the experimental data (Fig. 5). The value of the Freundlich index n (adsorption intensity) is 1.4–2.9 (e.g., n > 1), which indicates that the adsorbent MOF-199@GB favors benzene adsorption. In most cases, a strong π-π interaction is evident between the active sites on the adsorbent with the delocalized π electrons of the adsorbate molecule (Wu et al., 2020). The K_F for benzene adsorption onto MOF-199@GB decreased in the order 29.72 > 18.29 > 8.89 > 8.66 mg (g.MOF-199)$^{-1}$ $Pa^{-1/n}$ with increasing MOF-199 loading onto glass beads, in the order 1% < 3% < 10% < 20%. Likewise, the descending order of its n value (2.9 > 1.8 > 1.5 > 1.4) suggests that 1% MOF-199@GB offers superior adsorption of benzene compared with other MOF-199@GBs. The above decrease in K_F for benzene adsorption (1% > 3% > 10% > 20%) with increased MOF-199 loading onto GB can be accounted for by the decrease in available BET surface area (m^2 (g. MOF-199)$^{-1}$) such as 291 > 221 > 198 > 181, respectively).

3.5. Kinetic analysis of benzene adsorption onto MOF-199@GB

An analysis of benzene mass-uptake kinetics onto MOF-199@GB at a solid-gas interface is crucial for understanding the rate-controlling process of benzene adsorption onto MOF-199@GB vs. benzene vapor concentration in an inlet stream (Zhang, 2019). Here, the experimental data were fitted in a nonlinear mode to a pseudo-first-order model (PFOM, Eq. (11)) and pseudo-second-order model (PSOM, Eq. (12)) (Liu et al., 2021b; Wang and Guo, 2020). The PFOM represents physisorption, as it relies explicitly on the adsorption rate and the number of vacant sites available for adsorption (Carotenuto and Camerlingo, 2020). In contrast, the PSOM is used to fit chemisorption processes while being preferred for diffusion-controlled adsorption processes (Ho and McKay, 1999):

$$Q(t) = Q_{m1}[1 - \exp(-k_1 t)] \tag{11}$$

$$Q(t) = \frac{k_2 Q_{m2}^2 t}{1 + k_2 Q_{m2} t} \tag{12}$$

where Q(t) is the AC (mg g^{-1}) at a given breakthrough time of t (min). The theoretical maximum AC values (mg g^{-1}) predicted by PFOM and PSOM are Q_{m1} and Q_{m2}, respectively. Also, k_1 (min^{-1}) and k_2 (g mg^{-1} min^{-1}) imply the rate constants for PFOM and PSOM, respectively.

Kinetic rate constants derived from these two kinetic models along with their fitting correlations are reported in Tables 4 and 5. Fig. 6 shows the fitting curves between the experimental and predicted AC of benzene on the four MOF-199@GB adsorbents by PFOM and PSOM kinetic models at different inlet G-WS concentrations (1–100 ppm). Both PFOM and PSOM kinetic models can be used to accurately anticipate the experimental AC of benzene onto all MOF-199@GB adsorbents at all tested G-WS concentrations. However, PFOM is the best-fit model to describe benzene adsorption onto MOF-199@GB adsorbents, as it achieves the lowest error function (PD) value of 1%–18% and the highest R^2 value (>0.903). The Freundlich model offers a better fit than that of the Langmuir model, suggesting the dominance of multilayer adsorption of benzene onto MOF-199@GB. However, the significantly low observed AC (≤66 mg.(g.MOF-199)$^{-1}$) compared to the computed monolayer capacity (111 mg[g.MOF-199]$^{-1}$) at a small equilibrium P/P_0 of 0.00008 suggests that multilayer adsorption is highly improbable. We speculated that the affinity of MOF-199@GB for benzene uptake is controlled by monolayer, rather than multilayer, physisorption (Gutiérrez-Martínez et al., 2021).

As shown in Tables 4 and 1% MOF-199@GB exhibited the highest adsorption rates (k_1 and k_2) for benzene at all tested G-WS concentrations, with a descending order of 1% MOF-199@GB > 3% MOF-199@GB > 10% MOF-199@GB > 20% MOF-199@GB. This pattern indicates that 1% MOF-199@GB can offer better adsorption efficacy than those with other MOF-199 compositions. The faster adsorption rate of benzene by a 1% MOF-199@GB adsorbent could be explained by its higher BET surface-area-to-pore-volume relative to other adsorbents (Table 1). In addition, the PFOM rate constants (k_1) for benzene adsorption onto 1%, 3%, 10%, and 20% MOF-199@GB adsorbents decreased by 97%, 73%, 52%, and 72%, respectively, with a decrease in inlet concentration of benzene from 100 to 1 ppm (Table 4). This decrease in k_1 values can be attributed to mass-transfer resistance, which tends to increase with decreasing concentrations. As a result, benzene molecules are less likely to access internal active sorption sites within the cages of MOF-199 frameworks (Brosillon et al., 2001). These findings suggest that the diffusion/pore-filling mechanism is important in controlling the adsorption performance of MOF-199@GB toward benzene. Accordingly, the diffusivity (surface and pore diffusion) of benzene molecules through the cages of MOF-199@GB adsorbents is recognized as a rate-limiting step during the studied adsorption process.

3.6. Regeneration and reproducibility

The regeneration and reproducibility of the loaded adsorbent (MOF-199@GB) are indispensable prerequisites for real-world applications (Baker, 2016; Kumar et al., 2019; Lyu et al., 2022). To verify the

Table 4
Summary of the non-linear fitting results of the pseudo first-order kinetic model for adsorption of benzene onto MOF-199@GB.

Order	Adsorbent	Concentration ppm	Experimental apacity mg (g.MOF-199)$^{-1}$	PFOM Q_{m1} mg (g.MOF-199)$^{-1}$	k_1 (min^{-1})	R^2	RSSQ mg^2 (g.MOF-199)$^{-2}$	PD (%)
1	1% MOF-199@GB	1	20	15.18 ± 2.36	0.037 ± 0.007	0.994	0.4	13
2		5	23	21.21 ± 0.67	0.078 ± 0.037	0.903	12	4
3		10	25	24.58 ± 0.42	0.287 ± 0.016	0.989	18	10
4		50	50	42.16 ± 1.47	0.718 ± 0.084	0.956	134	10
5		100	66	63.85 ± 2.24	1.401 ± 0.125	0.987	50	5
6	3% MOF-199@GB	1	3	2.82 ± 0.02	0.188 ± 0.003	0.994	0.01	3
7		5	7	6.80 ± 0.08	0.443 ± 0.021	0.991	1.2	1
8		10	22	21.52 ± 0.28	0.201 ± 0.007	0.997	3	7
9		50	47	45.71 ± 0.64	0.442 ± 0.017	0.996	15	7
10		100	60	57.88 ± 1.37	0.694 ± 0.047	0.990	54	6
11	10% MOF-199@GB	1	2	1.29 ± 0.02	0.088 ± 0.004	0.993	0.03	9
12		5	5	4.75 ± 0.11	0.113 ± 0.007	0.990	0.6	14
13		10	9	9.45 ± 0.05	0.151 ± 0.002	0.999	0.2	4
14		50	26	26.65 ± 1.19	0.121 ± 0.012	0.982	24	18
15		100	40	39.09 ± 0.93	0.187 ± 0.011	0.995	15	13
16	20% MOF-199@GB	1	2	1.87 ± 0.01	0.052 ± 0.001	0.999	0.008	4
17		5	5	4.34 ± 0.07	0.064 ± 0.003	0.992	0.5	10
18		10	8	8.07 ± 0.09	0.061 ± 0.002	0.997	0.6	10
19		50	24	23.43 ± 0.24	0.113 ± 0.003	0.998	3	6
20		100	32	23.72 ± 0.29	0.190 ± 0.006	0.997	4	6

Table 5
Summary of the non-linear fitting results of the pseudo second-order kinetic model for adsorption of benzene onto MOF-199@GB.

Order	Adsorbent	Concentration	Experimental capacity	PSOM				
				Q_{m2}	k_2	R^2	RSSQ	PD
		ppm	mg (g.MOF-199)$^{-1}$	mg (g.MOF-199)$^{-1}$	(g.MOF-199) mg^{-1} min^{-1}		mg^2 (g.MOF-199)$^{-2}$	%
1	1% MOF-199@GB	1	20	19.49 ± 2.74	0.0016 ± 0.0005	0.994	0.5	18
2		5	23	22.38 ± 3.12	0.0007 ± 0.0002	0.955	51	28
3		10	25	28.94 ± 0.19	0.0114 ± 0.0003	0.999	1.5	4
4		50	50	48.72 ± 1.19	0.0183 ± 0.0019	0.988	37	5
5		100	66	83.22 ± 30	0.0153 ± 0.0018	0.993	24	3
6	3% MOF-199@GB	1	3	3.74 ± 0.10	0.0443 ± 0.0039	0.996	0.08	1
7		5	7	7.68 ± 0.09	0.0708 ± 0.0042	0.995	0.6	6
8		10	22	27.89 ± 0.24	0.0066 ± 0.0002	0.999	0.5	2
9		50	47	56.93 ± 0.59	0.0078 ± 0.0003	0.999	4	2
10		100	60	70.97 ± 0.66	0.0102 ± 0.0004	0.999	4	1
11	10% MOF-199@GB	1	2	1.66 ± 0.02	0.0509 ± 0.002	0.999	0.006	4
12		5	5	6.04 ± 0.12	0.0182 ± 0.0012	0.996	0.2	8
13		10	9	11.99 ± 0.16	0.0120 ± 0.0006	0.998	0.4	2
14		50	26	35.66 ± 1.72	0.0030 ± 0.0005	0.989	15	14
15		100	40	52.77 ± 1.63	0.0030 ± 0.0003	0.996	12	10
16	20% MOF-199@GB	1	2	2.47 ± 0.04	0.0186 ± 0.0011	0.997	0.04	12
17		5	5	5.51 ± 0.06	0.0113 ± 0.0005	0.999	0.1	5
18		10	8	10.49 ± 0.07	0.0053 ± 0.0001	0.9996	0.09	6
19		50	24	30.33 ± 0.2	0.0035 ± 0.0001	0.9996	0.6	1
20		100	32	30.28 ± 0.22	0.0059 ± 0.0002	0.9995	0.6	1

renewability of MOF-199@GB, tests were carried out in triplicate using 1% MOF-199@GB (as the best performer of MOF-199@GB) against 10 ppm benzene in N_2 using the same protocol as that for the benzene adsorption experiment (sections 2.5 and 2.6 and Table 2S). An appraisal of the regeneration performance of 1% MOF-199@GB is described in reference to the pristine MOF-199 and others.

After completing the sorption isotherm experiment, the spent 1% MOF-199@GB bed was thermally regenerated at 150 °C (temperature-swing desorption) for 3 h under a continuous N_2 stream (0.2 L atm min^{-1}). After each regeneration, an adsorption isotherm was obtained (three runs consisting of one before and two after each of the two regeneration cycles). As shown in Fig. 7a, BTV_{10} decreased by 20% (from 10 to 8 L atm (g.MOF-199)$^{-1}$) after the first regeneration cycle (Table 4S). The BTV_{10} AC decreased less significantly by 12% (from 26 to 22.7 mg [g.MOF-199]$^{-1}$) after the first regeneration, as shown in Fig. 7b.

After the second regeneration, the BTV_{10} of 1% MOF-199@GB underwent a further decrease of an additional 25% (from 8 to 6 L atm (g. MOF-199)$^{-1}$) as shown in Fig. 7a. This indicates that the spent 1% MOF-199@GB could not be fully regenerated after the two consecutive regeneration cycles as the BT10 AC decreased further by 10% (from 22.7 to 20.3 mg (g.MOF-199)$^{-1}$) as shown in Fig. 7a. The noticeable decrease of 22% in benzene BT10 AC of 1% MOF-199@GB (after two regenerations compared with the fresh sample) suggests that its renewability is marginal at best. Although a higher temperature would be required to fully regenerate the spent MOF-199@GB, temperature-swing regeneration of MOF-199@GB (e.g., >160 °C) is not recommended due to possible framework collapse of the MOF-199 and binder (PVA) melting.

The regeneration performance of 1% MOF-199@GB was compared with that of activated carbon, MOF-199, and a sorbent tube containing Carbopack C, B, and X toward benzene adsorbate, which was studied previously in our laboratory. A summary of the comparison is presented in Table 5S. Regeneration performance was assessed by fitting the 100% breakthrough capacity to Eq (13):

$$Q_n = Q_0[\exp(-k_r n)] \quad (13)$$

where n is the regeneration number (n = 0, fresh [unused]; n = 1, first regeneration; and n = 2, second regeneration), Q_0 is the capacity of the fresh (unused) adsorbent, Q_n is the capacity of the nth time regenerated adsorbent, and k_r is the regeneration decay constant. The regeneration decay constants at 0% relative humidity were: −0.25 (MOF-199), −0.126 (1% MOF-199@GB), −0.07 (activated carbon), and −0.0001 (mixed Carbopack CBX bed). The mixed Carbopack CBX bed sampling tube was reused 150 times with minimal performance loss in a series of experiments involving the loading of a mixture of benzene, toluene, isoprene, and nine terpenes in methanol for thermal desorption–based quantitation by gas chromatography (Ahn et al., 2016). The MOF-199 regeneration decay constants against benzene were relatively small, indicating satisfactory regeneration at least for one cycle (Anand et al., 2020b; Liu et al., 2021a). The activated carbon adsorbent could be regenerated satisfactorily up to 5 times (Liu et al., 2021b). The effect of humidity on activated carbon regeneration is potentially interesting as it can increase the AC of activated carbon, which is widely used and commercially regenerated using physical (thermal) and chemical (KOH) reactivation (Calgon Carbon Corporation, 2010). For example, in one of our previous studies, an increase in AC of activated carbon was evident after two regeneration cycles with a positive k_r value of 0.207 (Liu et al., 2021b). Here, freshly activated carbon was first loaded benzene at 5 Pa and 100% relative humidity (RH) and then at 0% RH for the first and second regenerations, respectively. The 1% MOF-199@GB exhibited superiority in terms of reusability, with a larger k_r (−0.126) (this study) compared to the pristine MOF-199 (k_r = −0.25) (Liu et al., 2021a).

As part of an additional QA to assess the reliability of our experimental approach, the reproducibility of our adsorption experiments was evaluated against 10 ppm benzene (Refer to section 2.3), Three tube samples (tube 1, tube 2, and tube 3) of 1% MOF-199@GB were prepared identically and tested individually to obtain triplicate data for comparison. All experiments were carried out by following the procedure for the benzene adsorption experiment as discussed in Sections 2.5 and 2.6. As can be seen in Fig. 8a, the maximum AC (BTV_{100}) differed by only 4% (29 vs. 30.6 mg [g.MOF-199]$^{-1}$) in tube 2 relative to tube 1 (Table 4S). This indicates that 1% MOF-199@GB can be reproduced to a large extent. However, the BTV_{10} changed by 5.5% (from 10 to 10.4 L atm [g. MOF-199]$^{-1}$) in tube 2 relative to tube 1, as shown in Fig. 8b.

The maximal AC (BTV_{100}) differed by only 3% (29 vs. 30 mg [g.MOF-199]$^{-1}$) in tube 3 relative to the tube 1, as shown in Fig. 8a. This indicates excellent reproducibility among the three different 1% MOF-199@GB beds. However, the BTV_{10} of 1% MOF-199@GB decreased by 6% (from 4.8 to 5 L atm [g.MOF-199]$^{-1}$) in tube 3 relative to the tube 1, as shown in Fig. 8b. The small change (≤5%) in benzene AC (in different tubes comparing three distinct fresh samples) confirms the reproducibility of the adsorption experiments when conducted with 1% MOF-199@GB. However, a noticeable reduction (≤6%) in BTV_{10} values over triplicate runs suggests a relatively significant variability in adsorption efficiency of 1% MOF-199@GB.

3.7. Benefits of MOF-199 bed modifications

The performance of MOF-199@GB (i.e., 1% MOF-199@GB) as an adsorbing system for gaseous benzene is compared to those reported previously in the literature. In 2020, we studied binding MOF-199 to a glass denuder to overcome operational challenges such as pressure drops

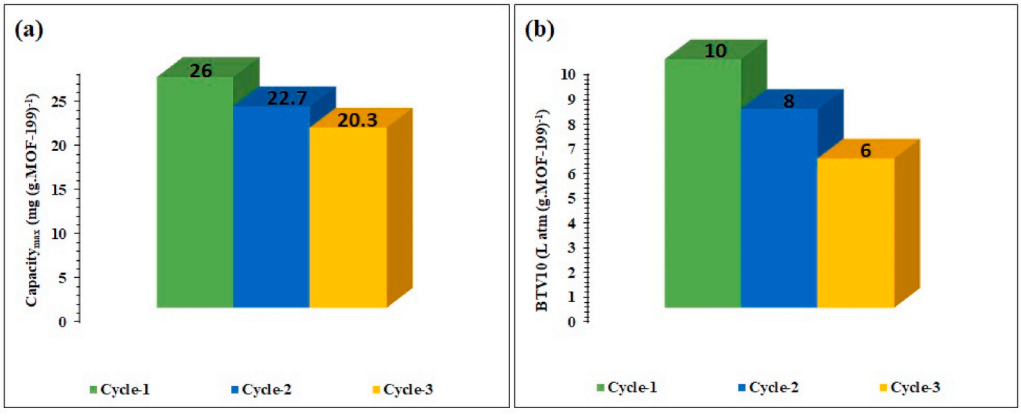

Fig. 7. Regeneration performance of 1% MOF-199@GB against benzene (10 ppm) after regenerating at 150 °C for 3 h in an uninterrupted N_2 stream (0.2 L atm min^{-1}) after each cycle of use: (a) capacity max (mg g^{-1}) and (b) BTV10 (L atm g^{-1}).

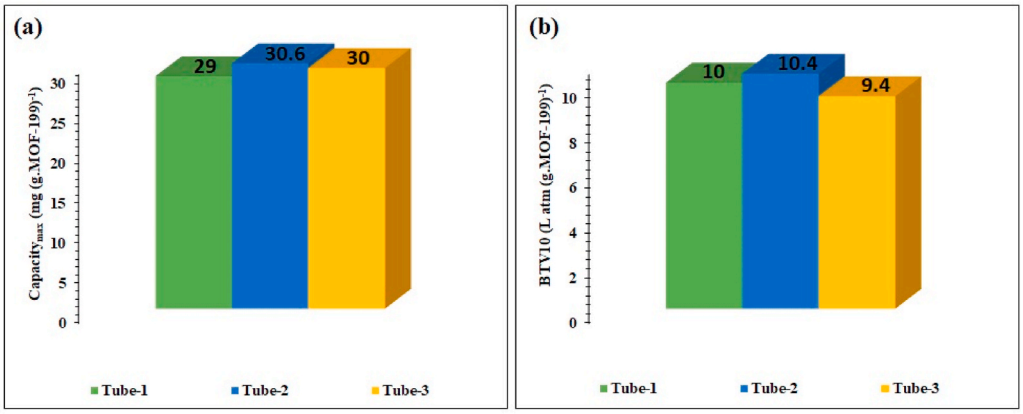

Fig. 8. Reproducibility of benzene (10 ppm) adsorption onto identically prepared 1% MOF-199@GB in three different tubes: (a) capacity max (mg g^{-1}) and (b) BTV10 (L atm g^{-1}).

Table 6
Performance comparison of benzene adsorption onto MOF-199 in conventional packed bed and alternatives. Conditions: 10 ppm, relative humidity = 0% and T = 298 K.

Order	Adsorbent	BTV10	Ads. Cap. at BTV10	Partition coefficient at BTV10	Max. Ads. Capacity	Pressure Drop (ΔP) % (atm)	Ref.
		L atm (g.MOF-199)$^{-1}$	mg (g.MOF-199)$^{-1}$	mol (kg.MOF-199)$^{-1}$Pa^{-1}	mg (g.MOF-199)$^{-1}$		
1	MOF-199 (Packed bed)	110	9	1.1	45	62.4	Anand et al. (2020b)
2	MOF-199 (Denuder)	2.4	0.053	0.007	12		Anand et al. (2020b)
3	1% MOF-199@GB	10	0.7	0.05	25	18.4	(This study)

in packed beds (Anand et al., 2020b). However, the benefit of the MOF@glass-tube denuder came at the cost of a four-fold reduction in maximum AC (Anand et al., 2020b). Here, we investigate the performance of a packed bed of MOF-199@GB for adsorptive removal of gaseous benzene in dry nitrogen.

In Table 6 and Table 5S, the results of relevant studies are summarized in relation to the design of MOF-199 sorbent beds for adsorptive removal of benzene. The adsorption performance of 1% MOF-199@GB against benzene is compared to that of 3%, 10%, and 20% MOF-199@GBs at near-ambient conditions (1 atm, 298 K) (Table 2). The performance of benzene adsorption onto 1% MOF-199@GB is comparable to that of a denuder (an alternative proposed in a previous study) in terms of BTV_{10}, AC (at BTV_{10}), PC (at BTV_{10}), and maximal AC. The comparison suggests the superiority of 1% MOF-199@GB over the previously proposed denuder, as shown by the fewest pressure drop issues. Specifically, if performances are compared at 1 Pa of benzene vapor in terms of BTV_{10}, 1% MOF-199@GB showed an approximately four-fold improvement in BTV_{10}, such as 10 L atm (g.MOF-199)$^{-1}$ over a denuder with 2.4 L atm (g.MOF-199)$^{-1}$. Apart from adsorption performance, our study also suggests that 10 g of 1% MOF-199@GB (0.1 g. MOF-199) is associated with a relatively low pressure drop of less than 20%, whereas 0.1 g of pristine MOF-199 in a packed bed experienced a pressure drop of 62.4%. This shows that 1% MOF-199@GB can efficiently overcome the problems of pressure resistance and drop associated with finely powered pristine MOF-199 in packed beds to a large extent (improved by a factor of 4). However, there was a two-fold reduction in the adsorption performance of 1% MOF-199@GB against 1 Pa benzene (25 mg [g.MOF-199]$^{-1}$) in terms of AC at 100% breakthrough relative to pristine MOF-199 (45 mg [g.MOF-199]$^{-1}$). This reduction in performance may reflect the alteration of pore texture in MOF-199 (reducing the active surface available for adsorption) due to the use of PVA as a binding agent in 1% MOF-199@GB. For details on pore texture, see Table 1).

4. Conclusions

Several types of MOFs as potent adsorbents for the efficient removal of VOCs have been studied. However, MOFs undergo a noticeable pressure drop when placed in a packed bed due to their fine particle size. To overcome this limitation, we explored the efficacy of MOF-based coated beads (MOF-199@GB). The applicability of MOF-199@GB was evaluated against different concentrations of benzene (1, 5, 10, 50 and 100 ppm) at ambient conditions. Our results emphasize the importance of the optimization procedures to assess the optimal amount of MOF component (MOF-199) bound in MOF-199@GB in terms of efficiency of adsorptive removal of benzene. The adsorption efficacy was evaluated in terms of BTV (L atm g^{-1}) at 10%, 50%, 90%, and 100% breakthrough, AC (mg g^{-1}), UR, and PC (mol kg^{-1} Pa^{-1}).

We found that the least-loaded 1% MOF-199 glass beads were more efficient than other compositions (3%, 10%, and 20%). This may reflect the undesirable consequences of using a PVA binder on the surface properties of MOF-199 (the active surface for adsorption) during preparation of MOF-199@GB relative to a packed bed. Based on these results, we recommend exploring superior alternatives to improve the adsorption performance of MOF-199@GB. Our reliability study also suggests the need for an automated synthesis method to warrant the reproducibility of MOF-199@GB to a certain extent.

Declaration of competing interest

The authors declare that they have no known competing financial interests or personal relationships that could have appeared to influence the work reported in this paper.

Acknowledgments

This work was supported by a grant from the National Research

Foundation of Korea (NRF) funded by the Ministry of Science and ITC (MSIT) of Korean government (Grant No: 2021R1A3B1068304). P.M.H. would like to thank the Research and Development Program of Ghent University Global Campus, Korea.

Appendix A. Supplementary data

Supplementary data to this article can be found online at https://doi.org/10.1016/j.envres.2021.112655.

References

Ahmed, A., et al., 2014. Macroporous metal–organic framework microparticles with improved liquid phase separation. J. Mater. Chem. 2, 9085–9090.

Ahn, J.-H., et al., 2016. Characterization of quality assurance properties of biogenic volatile organic compounds with an emphasis on the breakthrough behavior, recovery, and temporal stability. Microchem. J. 125, 142–150.

Al-Ghouti, M.A., Da'ana, D.A., 2020. Guidelines for the use and interpretation of adsorption isotherm models: a review. J. Hazard Mater. 393, 122383.

Anand, B., et al., 2020a. The effects of continuous- and stop-flow gas streams on adsorptive removal of benzene vapor using type – II covalent organic polymers. Environ. Res. 182, 109043.

Anand, B., et al., 2021. Proof of concept for CUK family metal-organic frameworks as environmentally-friendly adsorbents for benzene vapor. Environ. Pollut. 117491.

Anand, B., et al., 2020b. The potential utility of HKUST-1 for adsorptive removal of benzene vapor from gaseous streams using a denuder versus a packed-bed adsorption system. J. Clean. Prod. 275, 122359.

Andrew Lin, K.-Y., Hsieh, Y.-T., 2015. Copper-based metal organic framework (MOF), HKUST-1, as an efficient adsorbent to remove p-nitrophenol from water. J. Taiwan Inst. Chem. Eng. 50, 223–228.

Ashton, T.S., 1997. The Industrial Revolution 1760-1830. Oxford University Press.

Baker, M., 2016. Reproducibility crisis. Nature 533, 353–366.

Barea, E., et al., 2014. Toxic gas removal–metal–organic frameworks for the capture and degradation of toxic gases and vapours. Chem. Soc. Rev. 43, 5419–5430.

Brosillon, S., et al., 2001. Mass transfer in VOC adsorption on zeolite:experimental and theoretical breakthrough curves. Environ. Sci. Technol. 35, 3571–3575.

Calgon Carbon Corporation, 2010. Carbon Submittal for the ICS Excess Flow Treatment System. EPA, USA. https://semspub.epa.gov/work/05/424743.pdf.

Carotenuto, G., Camerlingo, C., 2020. Kinetic investigation of water physisorption on natural clinoptilolite at room temperature. Microporous Mesoporous Mater. 302, 110238.

CCDC, 2021. Access Structures. https://www.ccdc.cam.ac.uk/structures/Search?Compound=HKUST-1&DatabaseToSearch=Published, Accessed on May 20, 2021.

Chiang, Y.-C., et al., 2001. Effects of pore structure and temperature on VOC adsorption on activated carbon. Carbon 39, 523–534.

Dutta, T., et al., 2018a. Metal-organic framework and Tenax-TA as optimal sorbent mixture for concurrent GC-MS analysis of C1 to C5 carbonyl compounds. Sci. Rep. 8, 1–11.

Dutta, T., et al., 2018b. Metal-organic framework and Tenax-TA as optimal sorbent mixture for concurrent GC-MS analysis of C1 to C5 carbonyl compounds. Sci. Rep. 8, 5033.

Ergun, et al., 1952. Fluid flow through packed columns, vol. 48. Chem. Eng. Prog., pp. 89–94

Fan, C., et al., 2019. Sustainable synthesis of HKUST-1 and its composite by biocompatible ionic liquid for enhancing visible-light photocatalytic performance. J. Clean. Prod. 208, 353–362.

Farha, O.K., et al., 2012. Metal–organic framework materials with ultrahigh surface areas: is the sky the limit? J. Am. Chem. Soc. 134, 15016–15021.

Foo, K.Y., Hameed, B.H., 2010. Insights into the modeling of adsorption isotherm systems. Chem. Eng. J. 156, 2–10.

Freundlich, H., 1932. Of the adsorption of gases. Section II. Kinetics and energetics of gas adsorption. Introductory paper to section II. Trans. Faraday Soc. 28, 195–201.

Gaffney, T.R., 1996. Porous solids for air separation. Curr. Opin. Solid State Mater. Sci. 1, 69–75.

Gutiérrez-Martínez, J., et al., 2021. Fast benzene vapor capture by natural macroporous carbonized fibers improved with carbon nanostructures. Separ. Purif. Technol. 257, 117956.

Hendon, C.H., Walsh, A., 2015. Chemical principles underpinning the performance of the metal–organic framework HKUST-1. Chem. Sci. 6, 3674–3683.

Ho, Y.S., McKay, G., 1999. Pseudo-second order model for sorption processes. Process Biochem. 34, 451–465.

Holford, I., 1982. The comparative significance and utility of the Freundlich and Langmuir parameters for characterizing sorption and plant availability of phosphate in soils. Soil Res. 20, 233–242.

Hu, Z., et al., 2019. CO2 capture in metal–organic framework adsorbents: an engineering perspective. Adv. Sustain. Syst. 3, 1800080.

Khan, A., et al., 2018. The potential of biochar as sorptive media for removal of hazardous benzene in air. Chem. Eng. J. 361, 1576–1585.

Khan, N.A., et al., 2013. Adsorptive removal of hazardous materials using metal-organic frameworks (MOFs): a review. J. Hazard Mater. 244–245, 444–456.

Kim, K.-H., et al., 2017. Air ionization as a control technology for off-gas emissions of volatile organic compounds. Environ. Pollut. 225, 729–743.

Kim, K.H., Nguyen, H.T., 2007. Effects of injection volume change on gas chromatographic sensitivity determined with two contrasting calibration approaches for volatile organic compounds. J. Separ. Sci. 30, 367–374.

Kothiyal, G.P., et al., 2012. 9 - glass and glass-ceramics. In: Banerjee, S., Tyagi, A.K. (Eds.), Functional Materials. Elsevier, London, pp. 323–386.

Kumar, P., et al., 2019. Regeneration, degradation, and toxicity effect of MOFs: opportunities and challenges. Environ. Res. 176, 108488.

Langmuir, I., 1918. The adsorption of gases on plane surfaces of glass, mica and platinum. J. Am. Chem. Soc. 40, 1361–1403.

Leo, A., et al., 1971. Partition coefficients and their uses. Chem. Rev. 71, 525–616.

Liu, B., et al., 2021a. The dynamic competition in adsorption between gaseous benzene and moisture on metal-organic frameworks across their varying concentration levels. Chem. Eng. J. 421, 127813.

Liu, B., et al., 2021b. The competing role of moisture in adsorption of gaseous benzene on microporous carbon. Separ. Purif. Technol. 277, 119487.

Lyu, Y., et al., 2022. Scale-up reactivation of spent S-Zorb adsorbents for gasoline desulfurization. J. Hazard Mater. 423, 126903.

Macrae, C.F., et al., 2020. Mercury 4.0: from visualization to analysis, design and prediction. J. Appl. Crystallogr. 53, 226–235.

Minh, T.T., et al., 2018. Microwave synthesis and voltammetric simultaneous determination of paracetamol and caffeine using an MOF-199-based electrode. J. Mater. Sci. 53, 2453–2471.

Mohan, N., et al., 2009. Breakthrough of toluene vapours in granular activated carbon filled packed bed reactor. J. Hazard Mater. 168, 777–781.

Morita, M., et al., 2014. Why does the IR spectrum of hydroxide stretching vibration weaken with increase in hydration? Phys. Chem. Chem. Phys. 16, 23143–23149.

Moyo, M., et al., 2017. Biosorption of lead(II) by chemically modified Mangifera indica seed shells: adsorbent preparation, characterization and performance assessment. Process Saf. Environ. Protect. 111, 40–51.

Pandey, S.K., Kim, K.-H., 2009. Comparison of different calibration approaches in the application of thermal desorption technique: a test on gaseous reduced sulfur compounds. Microchem. J. 91, 40–46.

Perkin, H., 2003. The Origins of Modern English Society. Routledge.

Quiñones, I., Guiochon, G., 1996. Derivation and application of a jovanovic–freundlich isotherm model for single-component adsorption on heterogeneous surfaces. J. Colloid Interface Sci. 183, 57–67.

Raza, N., et al., 2017. Recent advances in titania-based composites for photocatalytic degradation of indoor volatile organic compounds. Asian J. Atmos. Environ. 11, 217–234.

Rosenberg, N., Birdzell, L.E., 1990. Science, technology and the Western miracle. Sci. Am. 263, 42–55.

Ross, C.F., 2012. 2.02 - headspace analysis. In: Pawliszyn, J. (Ed.), Comprehensive Sampling and Sample Preparation. Academic Press, Oxford, pp. 27–50.

Serna-Guerrero, R., Sayari, A., 2007. Applications of pore-expanded mesoporous silica. 7. Adsorption of volatile organic compounds. Environ. Sci. Technol. 41, 4761–4766.

Speight, J.G., 2018. Chapter 5 - sorption, dilution, and dissolution. In: Speight, J.G. (Ed.), Reaction Mechanisms in Environmental Engineering. Butterworth-Heinemann, pp. 165–201.

Spengler, J.D., Sexton, K., 1983. Indoor air pollution: a public health perspective. Science 221, 9.

Szanyi, J., et al., 2012. Well-studied Cu–BTC still serves surprises: evidence for facile Cu2+/Cu+ interchange. Phys. Chem. Chem. Phys. 14, 4383–4390.

Szulejko, J.E., et al., 2019. Seeking the most powerful and practical real-world sorbents for gaseous benzene as a representative volatile organic compound based on performance metrics. Separ. Purif. Technol. 212, 980–985.

Valizadeh, B., et al., 2018. Shape engineering of metal–organic frameworks. Polyhedron 145, 1–15.

Vellingiri, K., et al., 2017. Metal-organic frameworks for the adsorption of gaseous toluene under ambient temperature and pressure. Chem. Eng. J. 307, 1116–1126.

Vikrant, K., et al., 2019. Evidence for superiority of conventional adsorbents in the sorptive removal of gaseous benzene under real-world conditions: test of activated carbon against novel metal-organic frameworks. J. Clean. Prod. 235, 1090–1102.

Wang, J., Guo, X., 2020. Adsorption kinetic models: physical meanings, applications, and solving methods. J. Hazard Mater. 390, 122156.

Wilson, M., 1968. Indoor air pollution. Proc. Roy. Soc. Lond. Math. Phys. Sci. 307, 215–221.

Wu, Z., et al., 2020. Competitive adsorption of naphthalene and phenanthrene on walnut shell based activated carbon and the verification via theoretical calculation. RSC Adv. 10, 10703–10714.

Xiang, S., et al., 2009. Exceptionally high acetylene uptake in a microporous Metal−Organic framework with open metal sites. J. Am. Chem. Soc. 131, 12415–12419.

Zhang, J., 2019. Physical insights into kinetic models of adsorption. Separ. Purif. Technol. 229, 115832.

Zhang, W., et al., 2012. Comparison of dynamic adsorption/desorption characteristics of toluene on different porous materials. J. Environ. Sci. 24, 520–528.